ELSEVIER

Parameterization of iron and manganese cycling in the Black Sea suboxic and anoxic environment

Sergey Konovalov[a],*, Anatoliy Samodurov[a], Temel Oguz[b], Leonid Ivanov[c]

[a]*Marine Hydrophysical Institute, Ukrainian Academy of Sciences, Sevastopol 99011, Ukraine*
[b]*Middle East Technical University, Institute of Marine Sciences, Erdemli 33731, Icel, Turkey*
[c]*Woods Hole Group, Falmouth, MA 02540, USA*

Abstract

New and published data on the distribution and speciation of manganese and iron in seawater are analyzed to identify and parameterize major biogeochemical processes of their cycling within the suboxic ($\sim15.6 \leqslant \sigma_t \leqslant \sim16.2$) and anoxic layers ($\sigma_t \geqslant \sim16.2$) of the Black Sea. A steady-state transport-reaction model is applied to reveal layering and parameterize kinetics of redox and dissolution/precipitation processes. Previously published data on speciation of these elements in seawater are used to specify the nature of the transformations. Two particulate species of iron (Fe(III) hydroxide and Fe(II) sulfide) are necessary to adequately parameterize the vertical profile of suspended iron, while three particulate species (hydrous Mn(IV) oxide, Mn(II) sulfide, and Mn(II) carbonate) are necessary to describe the profile of suspended manganese. In addition to such processes as mixing and advection, precipitation, sinking, and dissolution of manganese carbonate are found to be essential in maintaining the observed vertical distribution of dissolved Mn(II). These results are used to interpret the observed difference in the form of vertical distribution for dissolved Mn(II) and Fe(II). Redox transformations of iron and manganese are coupled via oxidation of dissolved iron by sinking suspended manganese at $\sigma_t \sim 16.2 \pm 0.2\,\mathrm{kg\,m^{-3}}$. The particulate manganese, necessary for this reaction, is supplied through oxidation of dissolved Mn(II). The best agreement with observations is achieved when nitrate, rather than oxygen, is set to oxidize dissolved Mn(II) in the lower part of the suboxic layer ($\sim15.90 \leqslant \sigma_t \leqslant \sim16.2$). The results support the idea that, after sulfides of these metals are formed, they sink with particulate organic matter. The sinking rates of the particles and specific rates of individual redox and dissolved-particulate transformations have been estimated by fitting the vertical profile of the net rate.
© 2004 Elsevier Ltd. All rights reserved.

Key words: Black Sea; Suboxic and anoxic layer; Iron cycle; Manganese cycle; Biogeochemical parameterization; Inverse modeling

*Corresponding author. National Academy of Science of Ukraine, Marine Hydrophysical Institute, 2 Kapitanskaya St., Sevastopol 99000, Ukraine.

E-mail address: sergey@alpha.mhi.iuf.net (S. Konovalov).

1. Introduction

Iron (Fe) and manganese (Mn) are two major metals involved in redox cycling in oxic/anoxic marine environments. Classic studies of their transformations have been conducted in Framvaren Fjord (Landing and Westerlund, 1988), Cariaco Trench (Bacon et al., 1980; Zhang and Millero, 1993), the Baltic Sea (Kremling, 1983), and the Black Sea (Spencer and Brewer, 1971; Spencer et al., 1972; Lewis and Landing, 1991). In the Black Sea, sulfide, oxygen, nitrate, ammonium together with these metals form a complex redox system ultimately governing the location and structure of the suboxic–anoxic transition zone (Lewis and Landing, 1991; Tebo, 1991; Murray et al., 1995; Oguz et al., 2001). Individual redox transformations of manganese and iron have been addressed in several publications. In particular, the bacterial oxidation of dissolved Mn(II) by oxygen was studied by Tebo (1991); the formation of pyrite was addressed in Muramoto et al. (1991), Rickard (1997), and Rickard and Luther (1997). These studies have resulted in a sophisticated set of processes and parameters involved in the transformations. Some of these parameters have been used to simulate redox processes responsible for the consumption of the upward flux of sulfide in the Black Sea (Oguz et al., 2001). A set of processes that govern the overall budget and distribution of these elements throughout the suboxic ($\sim15.6 \leqslant \sigma_t \leqslant \sim16.2$) and anoxic ($\sigma_t \geqslant \sim16.2$) parts of the water column remain poorly resolved, and our understanding of these processes is still controversial.

In general, two basic processes describe the redox cycles of Fe and Mn in any oxic/anoxic water column. The first is the oxidation of dissolved Mn(II) and Fe(II) in the upper part of the water column generating particulate oxidized forms of these elements. The second process is the reduction and dissolution of sinking oxides and hydrous Fe(III) and Mn(III, IV) oxides. This process controls the inventory of dissolved reduced forms of these metals in the anoxic zone. In addition, sinking Fe(III) and Mn(III, IV) oxides react with sulfide in the absence of oxygen. The redox cycling of the metals is shaping the structure of their vertical distribution characterized by a distinctive interface separating the upper part of the water column, where oxidation dominates, from the lower part, where the major process is the reduction of Fe(III) and Mn(III, IV) oxides.

Murray et al. (1995, 1999) discussed a possible set of reactions involving iron and manganese redox cycling in the suboxic zone of the Black Sea and Oguz et al. (2001) presented a numerical model consisting of a simplified system of nitrogen and sulfur transformations catalyzed by redox cycling of manganese. These numerical simulations have shown that, in oxygen depleted waters, dissolved manganese reacts with nitrate to produce settling particulate manganese dioxide and nitrogen gas. In the model of Oguz et al. (2001), the upward flux of sulfide and ammonium was oxidized by sinking particulate manganese to form elemental sulfur, nitrogen gas, and dissolved manganese. Elemental sulfur was reduced back to sulfide by bacteria, whereas dissolved manganese further contributed to the process of nitrate reduction. Albeit simplified and idealized, the model was able to simulate the main biogeochemical features of the suboxic–anoxic transition zone of the Black Sea.

Lewis and Landing (1991) and Landing and Lewis (1991) published results of the most comprehensive studies on the biogeochemistry of manganese and iron in the Black Sea using the data collected during the 1988 *KNORR* cruise to the Black Sea, which provided a solid experimental basis to the investigation of solution speciation and solid-phase suspended particulate fractionation of manganese and iron. Modeling of Mn and Fe cycling in their work focused on providing justification to the fact that the Mn interface and Fe interface occur at different sigma-*t* levels and different depths. At the same time, their modeling efforts provided proof that the calculated removal rate of dissolved Mn in the suboxic zone agreed well with the [54]Mn potential bacterial oxidation rates. They calculated profiles of the vertical flux and first derivative of the flux of dissolved Mn(II) and Fe(II) but did not suggest an explanation of what could cause the differences between these profiles. No attempt has been made to quantify and/or parameterize processes that might be

responsible for the formation of the observed vertical structure of these two metals. That made impossible to directly utilize the data of Lewis and Landing (1991) for modeling, while the original observational data provided an extremely valuable basis, which was used in this work.

This study was conceived as a further development of modeling efforts of Lewis and Landing (1991). Using a different approach in estimating the mixing and advection terms in the transport-reaction equation we identify and parameterize the major redox and dissolved–suspended transformations of manganese and iron throughout the suboxic and anoxic parts of the Black Sea water column. The analysis intends to identify the predominant processes taking place in different layers and to estimate the specific rates of these processes and typical sinking rates of the particulate species. The present work is based on an inverse model inferring a set of parameters directly from the measured profiles of iron and manganese constituents. In a similar manner, the mixing and advection terms are defined from an inverse model based on conservation of heat, mass of salt, and mass of water for different layers of the Black Sea water column. These estimates serve as a basis for numerical simulation of iron and manganese cycling in the Black Sea water column.

2. Data and methods

2.1. Data

The profiles of dissolved Fe(II) and Mn(II) reconstructed in this work (Fig. 1) are based on measurements in the deep part of the Black Sea: at four stations occupied in the central and southern basin during the April–July 1988 R.V. *KNORR* expedition (Lewis and Landing, 1991) and at nine stations within the central and northern parts of the sea during the December 1994 and March–April 1995 cruises of R.V. *PROFESSOR KOLES-NIKOV* (Marine Hydrophysical Institute, Sevastopol, Ukraine). On the R.V. *PROFESSOR KOLESNIKOV*, dissolved Mn(II) was measured by the spectrophotometric formaldoxime method (Brewer and Spencer, 1971; Grasshoff et al., 1983).

Analysis of stored acidified samples from the R.V. *KNORR* were made with a Perkin-Elmer 5000 AAS with an HGA-400 graphite furnace and direct-injection GFAAS (Lewis and Landing, 1991). Dissolved manganese data obtained on different cruises by different analytical procedures (Fig. 1c and d) were found to be similar without any systematic difference in the layer above $\sigma_t \sim 16.5\,\mathrm{kg\,m^{-3}}$. At deeper levels, the difference was in fact less than 15% (Fig. 1c).

Dissolved Fe(II) from all cruises was measured by the ferrozine technique (Landing and Wester-lund, 1988). Although the vertical structures were similar (Fig. 1a and b), the maximum concentrations measured on board R.V. *PROFESSOR KOLESNIKOV* were about 50% lower than those measured from the R.V. *KNORR*. It will be demonstrated below that these differences are not a consequence of analytical errors but reflect interannual variability since the R.V. *PROFES-SOR KOLESNIKOV* data were collected 6–7 years later than the R.V. *KNORR* data. The data on suspended Fe and Mn (Fig. 1) were taken from Lewis and Landing (1991) for *KNORR* station BS3-6 located in the central part of the sea, away from the effects of continental margins.

The concentrations of Mn(II) and Fe(II) have a noticeable scatter when plotted against depth (Fig. 1). The scatter is much reduced when the density is used as the vertical coordinate. The use of density as the vertical coordinate has become a standard approach to present the Black Sea data since the early 1990s (Vinogradov and Nalbandov, 1990; Codispoti et al., 1991; Lewis and Landing (1991); Tugrul et al., 1992; Saydam et al., 1993; Buesseler et al., 1994; Murray et al., 1995; Konovalov et al., 1997; and others). The vertical distributions of dissolved Mn(II) and Fe(II) were approximated by exponential distributions to facilitate a more systematic data analysis. The vertical profile of suspended manganese was also smoothed below $\sigma_t \sim 16.2\,\mathrm{kg\,m^{-3}}$ to obtain a more uniform structure within the anoxic water column.

2.2. Methods

We define $\Phi^{\mathrm{diss}}(z)$ as the sum of vertical diffusive and advective fluxes of dissolved Mn(II) or Fe(II),
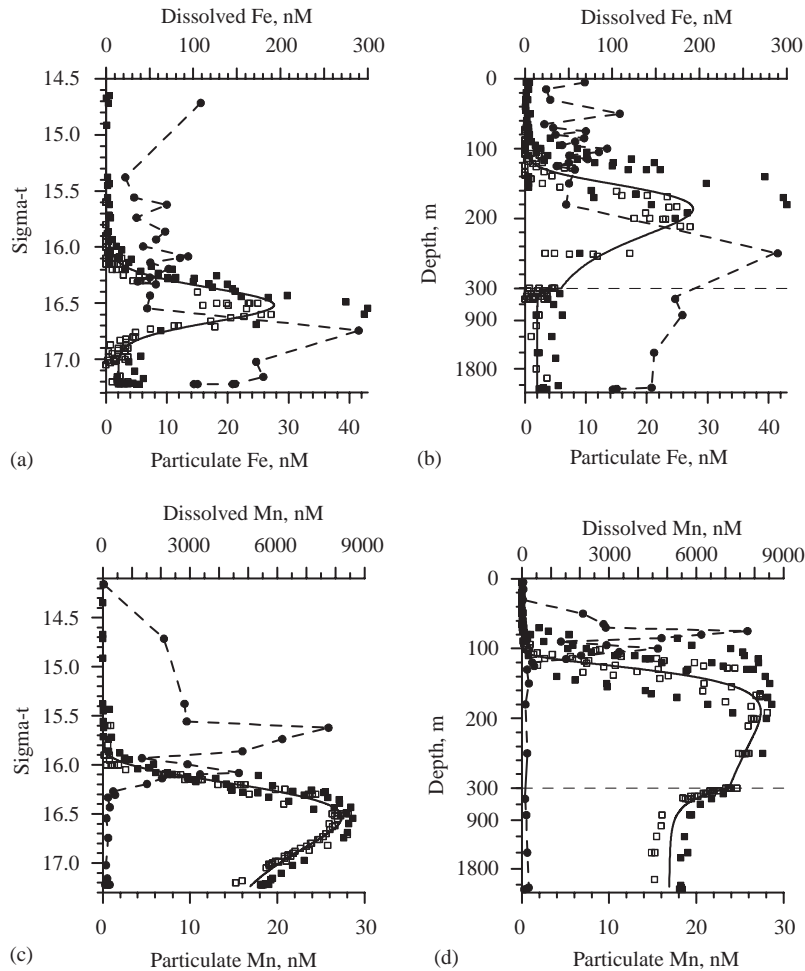
Fig. 1. Vertical distribution of particulate (circles, dashed line) and dissolved (squares, solid line) species of iron (a, b) and manganese (c, d) collected on board R.V. *KNORR* in 1988 (solid signs) and R.V. *PROFESSOR KOLESNIKOV* in 1994–1995 (open signs) plotted against density (a, c) and depth (b, d). (The depth scale is changed at 300 m.)

and $\Phi^{\text{susp}}(z)$ as the sum of n sinking fluxes of individual suspended forms of either manganese or iron expressed by

$$\Phi^{\text{diss}}(z) = -k(z)\,\frac{\partial C(z)}{\partial z} + w(z)\,C(z), \tag{1}$$

$$\Phi^{\text{susp}}(z) = \sum_{i=1}^{n} V_i C_i^{\text{susp}}(z), \tag{2}$$

where z is the vertical axis taken positive downward, $k(z)$ and $w(z)$ are the depth dependent coefficient of turbulent diffusion and vertical

velocity, respectively (Fig. 2), $C(z)$ is the concentration of dissolved manganese or iron derived from the smoothed profiles shown in Fig. 1, V_i is the sinking rate of an individual suspended constituent and $C_i^{\text{susp}}(z)$ is its concentration in the water column. Advection and turbulent diffusion are not considered for suspended constituents because they are negligible when compared to the sinking terms $V_i C_i^{\text{susp}}(z)$. The vertical distributions of $k(z)$ and $w(z)$ (Fig. 2) were found from a steady-state model of vertical exchange of heat and salt in the Black Sea. Model details are discussed in
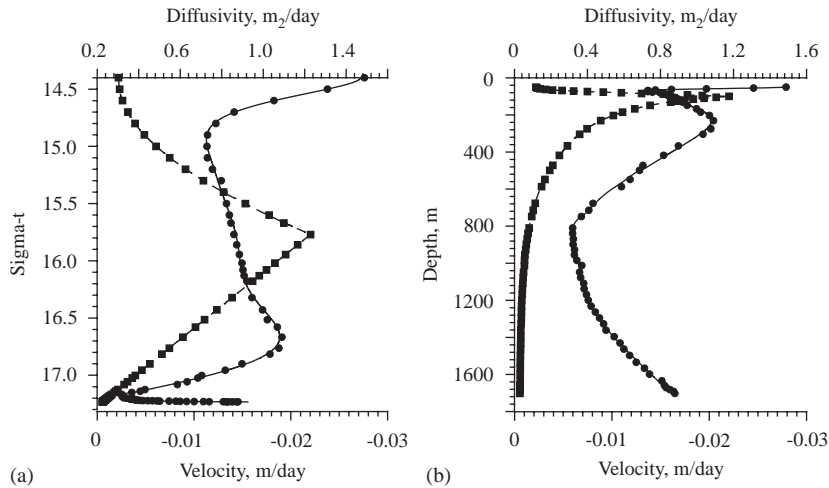
Fig. 2. Basin averaged vertical profiles of the vertical velocity (squares, dashed line) and diffusion coefficient (circles, solid line) derived from the vertical model by Ivanov and Samodurov (2001), plotted versus density (a) and depth (b).

Samodurov and Ivanov (1998) and Ivanov and Samodurov (2001). The major difference between basic model parameters, that is, distributions of $k(z)$ and $w(z)$, used here and in the work of Lewis and Landing (1991) is that in the model of Samodurov and Ivanov (1998) and Ivanov and Samodurov (2001) the advection and diffusion terms are not selected from a variety of 'suitable' choices but were determined from the balance of heat, mass of salt, and mass of water as a single possible combination. These profiles (Fig. 2) and other calculations in this work assume a basin-wide solution. The assumption is based on the isopycnal character of the distribution of major properties in the Black Sea. The depth scale used in this work is the basin-wide averaged depth corresponding to a number of sigma-t values.

The steady-state, one-dimensional advection–-diffusion–reaction equations can be expressed by

$$\frac{\partial \Phi^{\text{diss}}(z)}{\partial z} = R(z), \tag{3}$$

$$\frac{\partial \Phi_i^{\text{susp}}(z)}{\partial z} = R_i(z), \tag{4}$$

where the right-hand sides denote the net rate of biogeochemical production minus consumption (positive values indicate that production exceeds consumption) of dissolved constituents in Eq. (3)

and of suspended forms in Eq. (4). Conservation of the total flux of manganese and iron in the water column suggests

$$\sum_{i=1}^{n} R_i + R = 0 \tag{5}$$

implying that the consumption of one form results in the production of the other, either dissolved or suspended, if any other sources and sinks do not exist.

Lewis and Landing (1991) discussed the role of a lateral flux of dissolved Mn(II) in maintaining the structure of its vertical distribution. Shelf sediments may potentially be a source of dissolved Mn(II). Lewis and Landing (1991) showed that the vertical profile of dissolved Mn(II) was at a steady state from 1969 to 1988, which can be confirmed by way of comparison of the 1988 and 1995 data (Fig. 1), suggesting that the distribution of dissolved manganese was at steady state for almost 30 years. The data during this period of time were collected at different locations and in different seasons, but no distinct variations were revealed. At the same time, the flux of suspended manganese from the water column should balance all external sources to keep the distribution of manganese at a steady state. The maximum sedimentation rate (Lewis and Landing, 1991) is fairly small as

compared to the inventory of dissolved manganese, suggesting that any flux of manganese from sediments has a minor effect on the budget and cycling of manganese in the water column on a time scale from years to decades. Therefore, the flux of dissolved Mn(II) from the sediments was not considered in this work.

The integrated sum of Eqs. (3) and (4) implies

$$\sum_{i=1}^{n} V_i C_i^{\text{susp}}(z) + \Phi^{\text{diss}}(z) = \Phi_{\text{ext}}, \qquad (6)$$

where Φ_{ext} is an external flux of manganese or iron due to river runoff and atmospheric fallout. For convenience in future analysis, it may be presented as

$$\overline{V(z)} \sum_{i=1}^{n} C_i^{\text{susp}}(z) + \Phi^{\text{diss}}(z) = \Phi_{\text{ext}}, \qquad (7)$$

where $\overline{V(z)}$ is an average sinking rate of the total pool of suspended particles when suspended matter is not fractionated into individual constituents.

3. Dissolved manganese and iron fluxes

The fluxes calculated by Eq. (1) from the data in Fig. 1 indicate an upward transport of dissolved Mn(II) and Fe(II) from the anoxic zone into the suboxic layer (Fig. 3). The total upward Mn(II) flux for the area of the anoxic basin ($3 \times 10^{11} \, \text{m}^2$) attains its maximum value of about $2.71 \times 10^{10} \, \text{mol year}^{-1}$ at the suboxic–anoxic interface located around $\sigma_t \sim 16.2 \, \text{kg m}^{-3}$, at an average depth of about 120 m. It decreases upward and downward and approaches zero at 100 m ($\sigma_t \sim 15.7 \, \text{kg m}^{-3}$) within the suboxic layer and at depths below 1000 m. The total upward flux of Fe(II) is two orders of magnitude smaller and yields a peak value of $\sim 6.3 \times 10^8 \, \text{mol year}^{-1}$ at $\sim 150 \, \text{m}$ ($\sigma_t \sim 16.35 \, \text{kg m}^{-3}$), which is located 30 m and $0.15 \, \text{kg m}^{-3}$ below the maximum of the Mn(II) flux. It decreases at a much faster rate in both directions with an order of magnitude change in its intensity within the upper 30 m zone (toward $\sigma_t \sim 16.0 \, \text{kg m}^{-3}$) and the lower 50 m zone (toward $\sigma_t \sim 16.6 \, \text{kg m}^{-3}$). A narrow layer exists between approximately 200 and 300 m, below the depth where the upward transport of dissolved iron vanishes, in which the transport is directed downward at a maximum rate of $1.09 \times 10^8 \, \text{mol year}^{-1}$ near 230 m and $\sigma_t \sim 16.7 \, \text{kg m}^{-3}$. Our analysis suggests that these structures are insensitive to possible errors in the vertical Fe(II) and Mn(II) profiles.

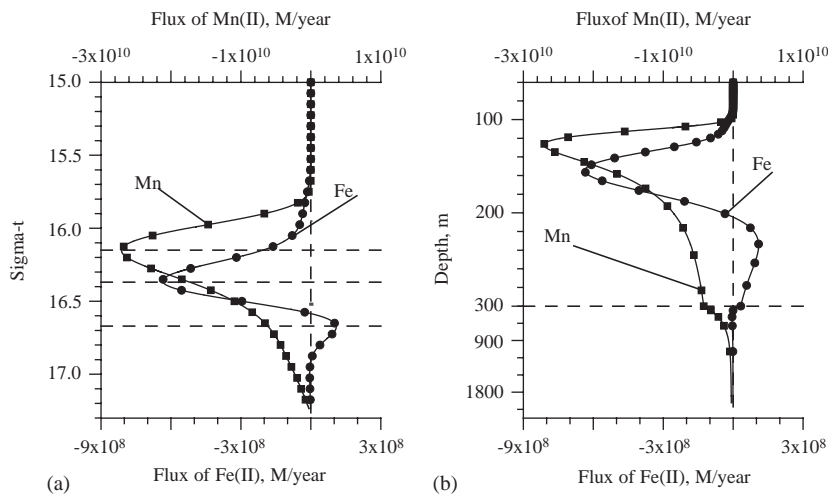Another indication of the difference between the manganese and iron cycles is given by the

Fig. 3. Total (integrated) vertical flux of dissolved iron (circles) and manganese (squares) plotted versus density (a) and depth (b). (Negative values mean that the flux is directed upward. The scale of the depth is changed at 300 m.)

residence times of dissolved Fe(II) and Mn(II). The inventory of dissolved manganese (3.33×10^{12} mol) and its total (deep-area integrated) upward flux (2.71×10^{10} mol year^{-1}) can be estimated from the data in Figs. 1 and 3, respectively, and the total area of the anoxic basin (3×10^{11} m^2). The turnover time of redox manganese cycling, as the ratio of the inventory to the flux, is about 123 years. This estimate is considerably different by its value and nature from the 19,000 years calculated by Lewis and Landing (1991) as the ratio of the inventory of dissolved Mn(II) to the sedimentation rate of particulate manganese. The value suggested by Lewis and Landing (1991) implies a mean residence time of manganese in the Black Sea. These values of the redox turnover time and mean residence time imply very intensive manganese cycling in the water column, when a big flux of dissolved Mn(II) from the anoxic zone is oxidized and reversed within the suboxic–anoxic transition layer, as compared to relatively small net import/export fluxes of manganese at the lateral boundaries of the Black Sea.

Similarly, for an estimated inventory and total upward flux of Fe(II) of 1.41×10^{10} mol and 6.36×10^8 mol year^{-1}, respectively, the time scale for iron redox cycling within the suboxic/anoxic transition layer is formally equal to 22 years. Muramoto et al. (1991) used 36×10^8 mol year^{-1} as the mean deep-area integrated sedimentation rate of iron sulfides and calculated the residence time for iron in the Black Sea waters to be 4 years. This value varies from 2.5 to 11 years when the extreme values of the sedimentation rate are used. All estimates suggest a considerably shorter lifetime of iron, when compared to the previous estimate of 19,000 years for manganese. Contrary to manganese, the time scale of redox cycling of iron is longer than its overall residence time in the water column. This implies that cycling of iron in the water column is basically a sequence of transformations from Fe(III) oxides to Fe(II) sulfides. The distribution and budget of iron essentially depend on the net supply from the atmosphere and river discharges (i.e. external sources), which are subject to large temporal variations on different time scales (Mitropolsky et al., 1982). In this manner, the changes in the vertical profile of Fe(II) that occurred between the R.V. *KNORR* 1988 and R.V. *PROFESSOR KOLESNIKOV* 1995 cruises are within the range of possible interannual variability.

4. Net production minus consumption rates

Further details on the characteristics of manganese and iron cycling can be obtained from the analysis of their net biogeochemical production minus consumption rates, R, computed according to Eq. (3). As shown in Fig. 4, the deep-area integrated rate of consumption exceeds the rate of production of Mn(II) above the onset of sulfide ($\sigma_t \approx 16.2$). Consumption increases upward to its maximum value of 1.7×10^9 mol m^{-1} year^{-1} at $\sigma_t \sim 15.95$ kg m^{-3} and decreases further at shallower depths within the suboxic layer. This structure implies a complex oxidation reaction kinetics expressed by its dependence on the concentration both of Mn(II) and its oxidant. Increasing oxidizer (either nitrate or oxygen) and decreasing Mn(II) concentrations toward upper levels, and their opposite trends toward lower levels of the suboxic zone imply a parabolic rate curve, as shown in Fig. 4. The profile of the net rate, R(Mn), further suggests production of Mn(II) inside the anoxic zone, below $\sigma_t \sim 16.2$ kg m^{-3}, due to reduction of sinking particulate Mn(III, IV). The production zone predominantly covers the layer between 125 and 300 m depths with the maximum production rate of $\sim 4.1 \times 10^8$ mol m^{-1} year^{-1} taking place at 145 m.

The profile of Fe(II) production minus consumption rate (Fig. 4) suggests consumption of some of the upward flux of dissolved iron above the onset of sulfide, where Fe(III) oxide is presumably produced. The rest of the upward flux of dissolved iron is consumed in the upper part of the anoxic layer above $\sigma_t \sim 16.35$ kg m^{-3}. The integrated maximum net consumption rate amounts to $\sim 2.2 \times 10^7$ mol m^{-1} year^{-1} and is much smaller than that of dissolved manganese. Its location in the depth range of 125–130 m is deeper than the depth of the maximum dissolved
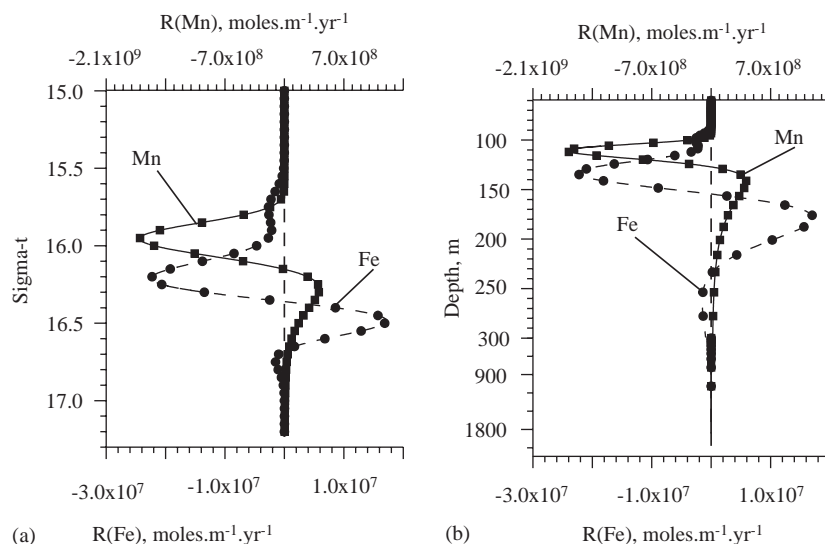
Fig. 4. Integrated vertical profile of the net production minus consumption rate of dissolved iron (R(Fe)) (circles, dashed line) and manganese (R(Mn)) (squares, solid line) plotted versus density (a) and depth (b). (Negative values mean that consumption exceeds production. The scale of the depth is changed at 300 m.)

manganese consumption rate, which is located in the suboxic zone, suggesting that different processes govern cycling of these metals. We suggest that the intimate relation between the maximum (minimum) dissolved manganese and iron, and net consumption (production) rates is compatible with the reaction

$$2Fe^{2+} + MnO_2 + 4H_2O = 2Fe(OH)_3 + Mn^{2+} + 2H^+. \tag{8}$$
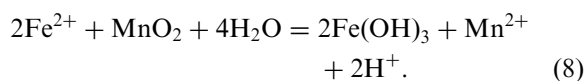
This reaction suggests that oxidation of Fe(II) may be coupled to sinking suspended Mn(IV) within the anoxic zone. This might also explain the observation that the concentration of suspended Fe remains constant in the anoxic layer from the onset of sulfide to $\sigma_t \sim 16.5\,kg\,m^{-3}$ (Fig. 1). Oxidation of Fe(II) by Mn(IV) has been investigated by Postma (1985, 2000) in sediments and laboratory experiments, but it has never been considered to be important for cycling of Mn and Fe in the suboxic–anoxic transition layer of the Black Sea.

Sinking Mn(IV) is, in fact, primarily spent to oxidize sulfide because the upward flux of iron can account for about 1% of the flux of sinking

Mn(IV). This makes redox cycling of iron tightly coupled to cycling of manganese, while the budget of manganese is quite independent from cycling of iron.

Deeper in the anoxic zone, a layer of net dissolved iron production is identified between approximately 150 m (at $\sigma_t \sim 16.35\,kg\,m^{-3}$) and 230 m (at $\sigma_t \sim 16.75\,kg\,m^{-3}$) with a maximum rate of $\sim 1.7 \times 10^7\,mol\,m^{-1}\,year^{-1}$. The layer occurs is due to reduction and dissolution of sinking suspended Fe(III). A small net consumption of dissolved iron below 230 m may also be explained by fast production of iron sulfides (Rickard, 1997).

5. Sinking rates for particulate manganese and iron

The values of the average sinking rates of particulate manganese and iron can be calculated from Eq. (7) and their concentrations and dissolved fluxes (see Figs. 1 and 3). The value of external source is set to $0.43\,\mu mol\,m^{-2}\,d^{-1}$ for manganese (Lewis and Landing, 1991) and $35\,\mu mol\,m^{-2}\,d^{-1}$ for iron (Muramoto et al., 1991). The computed profile of the sinking rate
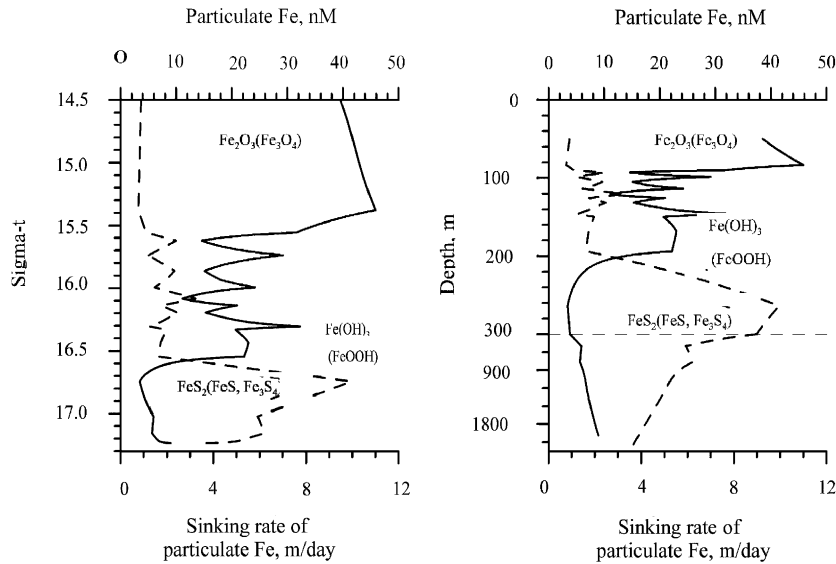
Fig. 5. Vertical profiles of particulate iron by Lewis and Landing (1991) (dashed line) and the calculated vertical profile of the rate of sinking (solid line) for the observed distribution of particulate iron. (All calculations are based on utilization of Eq. (7).)

of particulate iron (Fig. 5) attains a value of $\sim 5 \pm 1\,\mathrm{m\,d^{-1}}$ within the suboxic layer and the upper part of the anoxic zone above $\sim 200\,\mathrm{m}$ at $\sigma_t \sim 16.5\,\mathrm{kg\,m^{-3}}$. It then sharply decreases to $\sim 1\,\mathrm{m\,d^{-1}}$ near $250\,\mathrm{m}$ and $\sigma_t \sim 16.7\,\mathrm{kg\,m^{-3}}$, followed by a gradual increase up to $\sim 2\,\mathrm{m\,d^{-1}}$ near the bottom. The sinking rate of particulate manganese (Fig. 6), on the other hand, undergoes more pronounced variations in the water column. Its typical value of $15\,\mathrm{m\,d^{-1}}$ near the suboxic–anoxic interface around $\sigma_t \sim 16.0\,\mathrm{kg\,m^{-3}}$, $100\,\mathrm{m}$, sharply increases to a value of $200\,\mathrm{m\,d^{-1}}$ at $\sigma_t \sim 16.4\,\mathrm{kg\,m^{-3}}$, $150\,\mathrm{m}$. It then decreases almost linearly with respect to density toward the bottom (Fig. 6a). When plotted with respect to depth (Fig. 6b), these variations show different trends at different layers of the water column. The most dramatic changes occur within the 150-m thick layer right below its maximum value, where it decreases to $\sim 75\,\mathrm{m\,d^{-1}}$ at $300\,\mathrm{m}$. Thereafter, it decreases to $\sim 10\,\mathrm{m\,d^{-1}}$ within the next $700\,\mathrm{m}$ layer, and finally to $\leqslant 5\,\mathrm{m\,d^{-1}}$ within the deepest part of the water column. The chemical fractionation analyses by Lewis and Landing (1991) suggested suspended forms of manganese and iron in the deep waters are primarily in the form

of sulfides. The fact that the fluxes of iron, particulate organic matter and sulfide are highly correlated in deep waters (Muramoto et al., 1991) implies generation of iron and manganese sulfides in flocks or aggregates of sinking particular organic matter. Our estimates of the rate of sinking (Figs. 5 and 6) are comparable with the POM sinking rates of $0.8\,\mathrm{m\,d^{-1}}$ derived from sediment trap data reported by Karl and Knauer (1991).

Particulate iron and manganese are dominated by their oxides within the upper part of the anoxic waters (Lewis and Landing, 1991). Our sinking rate estimates of the order of $10\,\mathrm{m\,d^{-1}}$ near the onset of sulfide layer are typical for amorphous forms of particulate iron and manganese (Oguz et al., 2001; Diercks and Asper, 1997). The sinking rates for manganese on the order of $100\,\mathrm{m\,d^{-1}}$, on the other hand, indicate the presence of another particulate form at intermediate depths of the water column. This might be $MnCO_3$ as suggested by Spencer and Brewer (1971). Landing and Lewis (1991) argued for under-saturation of the Black Sea waters with respect to $MnCO_3$, but they applied equilibrium thermodynamic modeling and did not consider any
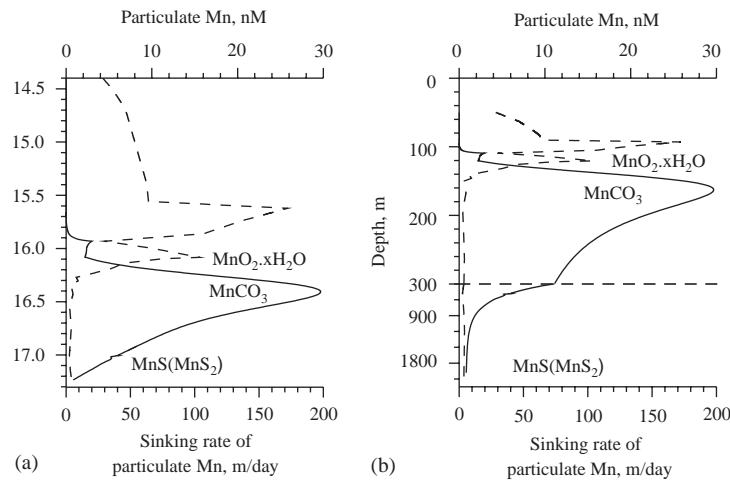
Fig. 6. Vertical profiles of particulate manganese by Lewis and Landing (1991) (dashed line) and the calculated vertical profile of the rate of sinking (solid line) for the observed distribution of particulate manganese. (All calculations are based on utilization of Eq. (7).)

heterogeneous processes. This type of modeling crucially depends on the quality of the published solubility products and ability to precisely calculate the activity of ions, rather than their concentrations. Biogeochemical cycling in marine environments is kinetically controlled, and a heterogeneous process of reduction of sinking particulate Mn oxide can easily result in a locally high concentration of dissolved Mn(II) that would be enough to precipitate $MnCO_3$. Thus, iron cycling within the suboxic–anoxic waters of the Black Sea requires consideration of its dissolved form, Fe(III) hydroxide in the suboxic layer and the upper part of the anoxic zone, and Fe(II) sulfide within the rest of the anoxic water column. Manganese cycling, on the other hand, requires consideration of Mn(II) carbonate in addition to Mn(IV) oxide and Mn(II) sulfide. In our subsequent analysis, we set the sinking rate of Fe(III) hydroxide to $5.3\,\mathrm{m\,d^{-1}}$ as a mean value between $\sigma_t \sim 15.5$ and $\sim 16.5\,\mathrm{kg\,m^{-3}}$, and of Fe(II) sulfide to $0.8\,\mathrm{m\,d^{-1}}$. The corresponding value for hydrous Mn(IV) oxide is taken as $14.7\,\mathrm{m\,d^{-1}}$ and for Mn(II) sulfide $0.8\,\mathrm{m\,d^{-1}}$. We also assume that the maximum of $198\,\mathrm{m\,d^{-1}}$ for the sinking rate of particulate manganese (Fig. 6) is the sinking rate of Mn(II) carbonate.

6. Fractionation of particulate manganese and iron

Assuming that iron hydroxide and iron sulfide predominantly exist above $\sigma_t \sim 16.55\,\mathrm{kg\,m^{-3}}$ and below $\sigma_t \sim 16.75\,\mathrm{kg\,m^{-3}}$, respectively, and that changes in the rate of sinking of particulate iron from $\sigma_t \sim 16.55$ to $16.75\,\mathrm{kg\,m^{-3}}$ are due to changes in the ratio of iron hydroxide to iron sulfide, Eq. (6) for this layer can be expressed as

$$C_{Fe(OH)_3}(z)\, V_{Fe(OH)_3} + C_{FeS_2}(z)\, V_{FeS_2} + \Phi_{Fe(II)}(z)$$
$$= \Phi_{ext}. \tag{9a}$$

This expression together with

$$C_{Fe(OH)_3}(z) = C_{Fe_{susp}}(z) - C_{FeS_2}(z) \tag{9b}$$

can be solved for concentrations of iron hydroxide $C_{Fe(OH)_3}(z)$ and iron sulfide $C_{FeS_2}(z)$. Their vertical profiles and individual contributions to the total particulate iron inventory are shown in Fig. 7 as percent and Fig. 8 as concentration. Fig. 7 reveals that the hydroxide contribution declines rapidly from 195 to 265 m, while the sulfide contribution increases. They attain equal contributions at $\sigma_t \sim 16.6\,\mathrm{kg\,m^{-3}}$. Below $\sigma_t \sim 16.75\,\mathrm{kg\,m^{-3}}$, the concentration $C_{FeS_2}(z)$ decreases gradually (Fig. 8). This decrease might reflect transformation between different iron sulfide species, which cannot

be resolved with the existing data. Variations in the sinking rate of POM and temporal variations in the external flux of iron may also contribute to the near-bottom variations of iron sulfide concentrations.

Similarly, suspended manganese can be partitioned into hydrous Mn(IV) oxide and Mn(II) carbonate forms within the layer of $\sigma_t \sim 16.1$ to $\sim 16.4\,\mathrm{kg\,m^{-3}}$, and its carbonate and sulfide forms below $\sigma_t \sim 16.4\,\mathrm{kg\,m^{-3}}$. Then, we can write for the layer above $\sigma_t = 16.4\,\mathrm{kg\,m^{-3}}$

$$C_{\mathrm{MnO_2}}(z)V_{\mathrm{MnO_2}} + C_{\mathrm{MnCO_3}}(z)V_{\mathrm{MnCO_3}} + \Phi_{\mathrm{Mn(II)}}(z) = \Phi_{\mathrm{ext}}, \tag{10a}$$

$$C_{\mathrm{MnO_2}}(z) = C_{\mathrm{Mn_{susp}}}(z) - C_{\mathrm{MnCO_3}}(z) \tag{10b}$$

and for the layer below $\sigma_t = 16.4\,\mathrm{kg\,m^{-3}}$

$$C_{\mathrm{MnCO_3}}(z)\,V_{\mathrm{MnCO_3}} + C_{\mathrm{MnS_2}}(z)\,V_{\mathrm{MnS_2}} + \Phi_{\mathrm{Mn(II)}}(z) = \Phi_{\mathrm{ext}}, \tag{11a}$$
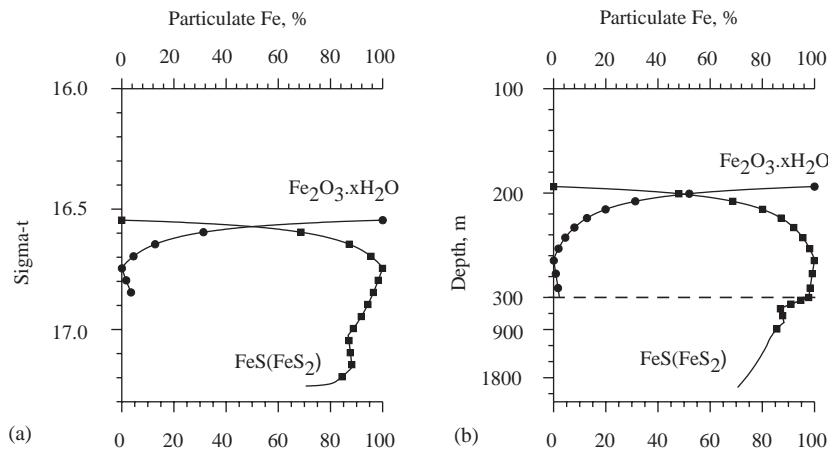

Fig. 7. Partitioning of iron hydroxide (circles) and iron sulfide (squares) as percent of the total particulate iron.
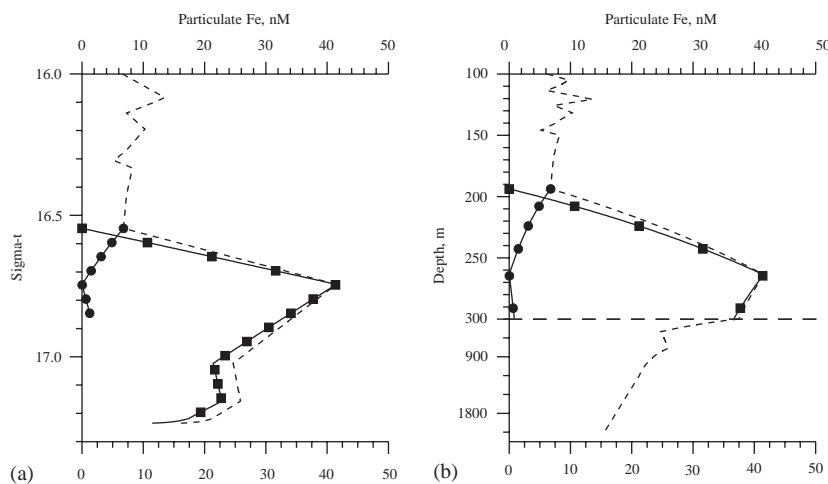

Fig. 8. Vertical distribution of the concentration of iron hydroxide (circles, solid line), iron sulfide (squares, solid line), and total particulate iron (dashed line).

$$C_{MnCO_3} = C_{Mn_{susp}} - C_{MnS_2}. \qquad (11b)$$

Solutions to these equations are shown in Figs. 9 and 10. While hydrous Mn(IV) oxide dominates the layer near the onset of sulfide, manganese sulfide appears increasingly toward the bottom. The concentration of manganese carbonate is low throughout the water column (Fig. 10), but it exceeds 50% of total suspended manganese from $\sigma_t \sim 16.25$ to $\sim 16.7 \, \text{kg m}^{-3}$ (Fig. 9) making sus-

pended carbonate very important for the overall cycle of manganese.

7. Reaction kinetics for iron cycling

A set of specific reactions for production and transformations of the particulate and dissolved forms of iron and manganese discussed in the previous sections is suggested here. Beside oxidation of dissolved Fe(II) by suspended Mn(IV)
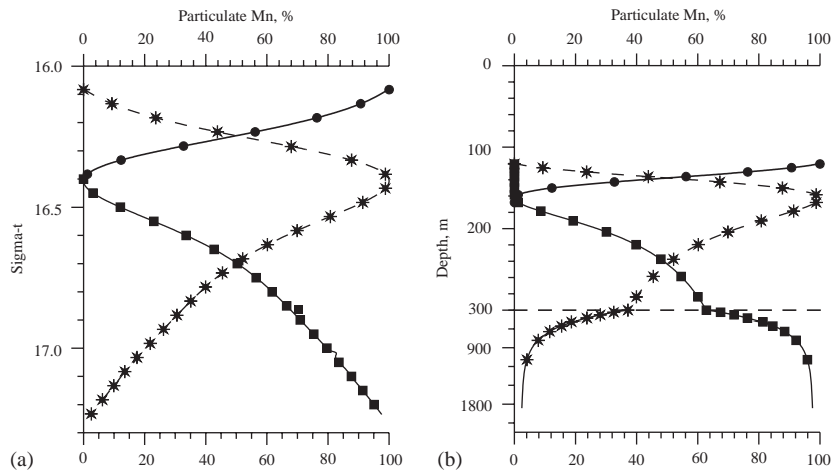

Fig. 9. Partitioning of manganese oxide (circles, thin solid line), manganese carbonate (stars, dashed line), and manganese sulfide (squares, solid line) as percent of the total particulate manganese.
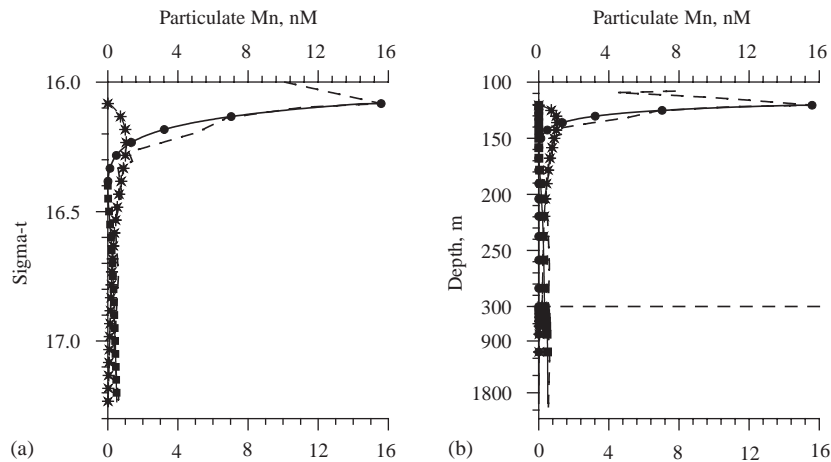

Fig. 10. Vertical distribution of the concentration of manganese oxide (circles, thin solid line), manganese carbonate (stars, dashed line), manganese sulfide (squares, solid line), and total particulate manganese (thin dashed line).

oxide (Eq. (8)), cycling of iron involves reduction of Fe(III) hydroxide to dissolved Fe(II) by sulfide in the upper part of the anoxic zone

$$8Fe(OH)_3 + HS^- + 15H^+ = 8Fe^{2+} + SO_4^{2-}$$
$$+20H_2O \qquad (12a)$$
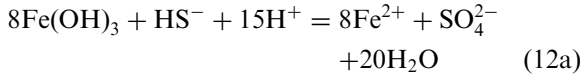
and reaction of dissolved Fe(II) with hydrogen sulfide to form pyrite (FeS$_2$) at deeper levels

$$Fe^{2+} + 2HS^- = FeS_2 + H_2. \qquad (12b)$$
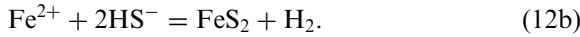
According to the principles of formal chemical kinetics, the rate of these reactions can be defined by

$$R_1^{Fe} = K_1^{Fe} C_{Fe^{2+}} C_{MnO_2}^{1/2} : \text{ oxidation of}$$
$$Fe(II) \text{ (Eq. (8)),} \qquad (13a)$$

$$R_2^{Fe} = K_2^{Fe} C_{Fe(OH)_3} C_{HS^-}^{1/8} : \text{ reduction of}$$
$$Fe(III) \text{ (Eq. (12a)),} \qquad (13b)$$

$$R_3^{Fe} = K_3^{Fe} C_{Fe^{2+}} C_{HS^-}^2 \approx K_3^{Fe} C_{Fe^{2+}} : \text{ production of}$$
$$FeS_2 \text{ (Eq. (12b)),} \qquad (13c)$$

The approximation suggested in Eq. (13c) assumes that concentrations of hydrogen sulfide remain at a steady state within the deeper levels of the water column.

The suggested Eqs. (13a)–(13c) do not represent the actual mechanisms of the considered processes but they are rather a formal description of the rate law. Both the species term, whose concentration appears in the rate law, and exponents need not be a reactant or product in the overall stoichiometric reaction (Stumm and Morgan, 1996). These values are chosen to keep the specific rate of processes to a steady state as close as possible.

Following Eq. (4), the equations describing the budget of the individual particulate iron species are then expressed by

$$V_{Fe(OH)_3} \frac{\partial C_{Fe(OH)_3}(z)}{\partial z} = K_1^{Fe} C_{Fe^{2+}}(z) C_{MnO_2}^{1/2}(z),$$
$$(14a)$$

$$V_{Fe(OH)_3} \frac{\partial C_{Fe(OH)_3}(z)}{\partial z} = K_1^{Fe} C_{Fe^{2+}}(z) C_{MnO_2}^{1/2}(z)$$
$$- K_2^{Fe} C_{Fe(OH)_3}(z) C_{HS^-}^{1/8}(z),$$
$$(14b)$$

$$V_{FeS_2} \frac{\partial C_{FeS_2}(z)}{\partial z} = K_3^{Fe} C_{Fe^{2+}}(z). \qquad (14c)$$

While Eq. (14a) applies for the suboxic layer, Eqs. (14b) and (14c) describe the balance for the upper part of the anoxic layer near the onset of sulfide and intermediate-deep layers of the water column, respectively. Given the concentrations and sinking rates as described in the previous sections, these equations are solved for unknown rate constants K_1^{Fe}, K_2^{Fe} and K_3^{Fe} representing the specific rate of Fe(III) hydroxide production, hydroxide dissolution and iron sulfide production, respectively. The value of K_3^{Fe} varies between 0.0034 and 0.0049 d^{-1}. Its mean value is 0.0038 ± 0.004 d^{-1}. The mean values of other rate constants are determined by least-squares fitting as $K_1^{Fe} = 0.023$ d^{-1} nmol$^{-1/2}$ and $K_2^{Fe} = 0.051$ d^{-1} nmol$^{-1/8}$ (Table 1).

These parameterizations were tested by simulating the vertical profile of the total suspended iron

Table 1
Average rates of sinking and specific rates of reactions driving cycling of iron and manganese in the suboxic–anoxic water column of the Black Sea

Parameter	Value
Manganese	
K_1^{Mn} of Mn(IV) oxide production	0.00046 d^{-1} nmol$^{-1.4}$
V_1^{Mn} of Mn(IV) oxide sinking	14.7 m d^{-1}
K_2^{Mn} of Mn(IV) oxide dissolution	2.3 d^{-1}
K_3^{Mn} of Mn(II) carbonate production	2.7 d^{-1}
V_2^{Mn} of Mn(II) carbonate sinking	198 m d^{-1}
K_4^{Mn} of Mn(II) carbonate dissolution	3.8 d^{-1} nmol$^{-0.7}$
K_5^{Mn} of Mn(II) sulfide production	0.014 d^{-1} nmol$^{-0.7}$
V_3^{Mn} of Mn(II) sulfide sinking	0.8 m d^{-1}
Iron	
K_1^{Fe} of Fe(III) hydroxide production	0.023 d^{-1} nmol$^{-0.5}$
V_1^{Fe} of Fe(III) hydroxide sinking	5.3 m d^{-1}
K_2^{Fe} of Fe(III) hydroxide dissolution	0.051 d^{-1} nmol$^{-0.125}$
K_3^{Fe} of Fe(II) sulfide production	0.0038 d^{-1}
V_2^{Fe} of Fe(II) sulfide sinking	0.8 m d^{-1}
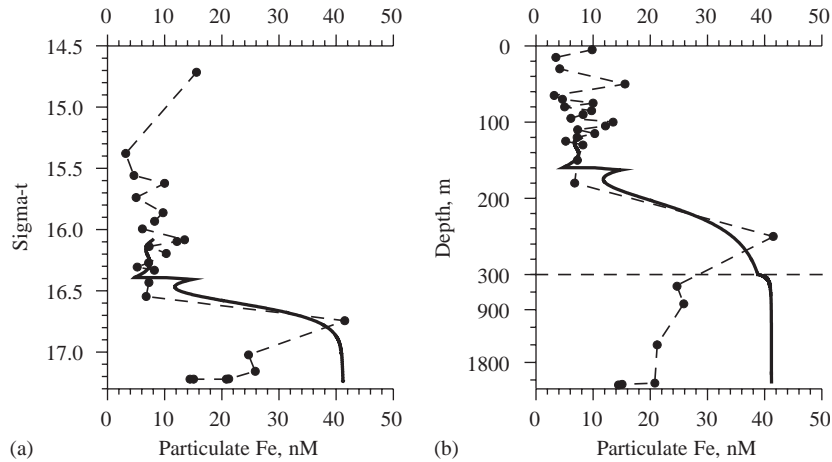
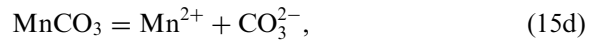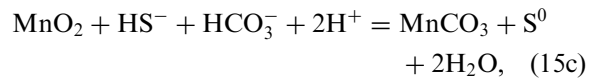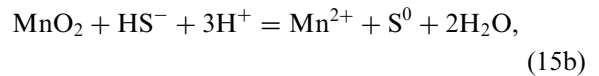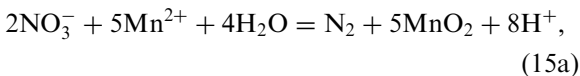Fig. 11. Observed (dashed line) and calculated (solid line) vertical distribution of total particulate iron.

concentration (Fig. 11) using analytical data for dissolved Fe(II), external flux of iron and the parameterizations given by Eq. (14). The computed and observed profiles of particulate iron compare reasonably well, from the onset of the anoxic layer to a depth of about 300 m and $\sigma_t = 16.75$. At greater depth the computed profile is vertically uniform, while the observed profile exhibits a gradual decline. This difference is related to the simplifications and assumptions (such as a vertically constant sinking rate and temporarily constant external flux) introduced during the analysis of the iron cycle.

8. Reaction kinetics for manganese cycling

The reactions proposed to control manganese cycling include (i) oxidation of dissolved manganese in the suboxic layer by nitrate (Eq. (15a)), (ii) reduction of Mn(IV) oxide by sulfide (Eq. (15b)) followed by formation of Mn(II) carbonate in the upper part of the anoxic layer (Eq. (15c)), (iii) dissolution of manganese carbonate in the deeper layers (Eq. (15d)) and formation of manganese sulfide (Eq. (15e)).

$$2NO_3^- + 5Mn^{2+} + 4H_2O = N_2 + 5MnO_2 + 8H^+, \tag{15a}$$

$$MnO_2 + HS^- + 3H^+ = Mn^{2+} + S^0 + 2H_2O, \tag{15b}$$

$$MnO_2 + HS^- + HCO_3^- + 2H^+ = MnCO_3 + S^0 + 2H_2O, \tag{15c}$$

$$MnCO_3 = Mn^{2+} + CO_3^{2-}, \tag{15d}$$

$$Mn^{2+} + 2HS^- = MnS_2 + H_2. \tag{15e}$$
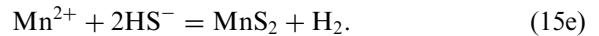
The kinetics of these reactions are formally expressed as follows:

$$R_1^{Mn} = K_1^{Mn} C_{Mn^{2+}} C_{NO_3^-}^{2/5} C_{MnO_2} : \text{ oxidation of Mn(II)}$$
$$(\text{Eq. (15a)}), \tag{16a}$$

$$R_2^{Mn} = K_2^{Mn} C_{MnO_2} : \text{ reduction of Mn(IV)}$$
$$(\text{Eq. (15b)}), \tag{16b}$$

$$R_3^{Mn} = K_3^{Mn} C_{MnO_2} : \text{ production of Mn(II)}$$
$$\text{carbonate (Eq. (15c)),} \tag{16c}$$

$$R_4^{Mn} = K_4^{Mn}(C_{MnCO_3})^{1.7} : \text{ dissolution of Mn(II)}$$
$$\text{carbonate (Eq. (15d)),} \tag{16d}$$

$$R_5^{Mn} = K_5^{Mn}(C_{MnCO_3})^{1.7} : \text{ production of Mn(II)}$$
$$\text{sulfide (Eq. (15e)).} \tag{16e}$$

As in the case of iron, the equations can be written for manganese as

$$\frac{\partial \Phi_{\text{diss}}^{\text{Mn(II)}}(z)}{\partial z} = -K_1^{\text{Mn}}\, C_{\text{Mn}^{2+}}(z)\, C_{\text{NO}_3^-}^{2/5}(z)\, C_{\text{MnO}_2}(z), \tag{17a}$$

$$V_{\text{MnO}_2}\, \frac{\partial C_{\text{MnO}_2}(z)}{\partial z} = -K_2^{\text{Mn}}\, C_{\text{MnO}_2}(z), \tag{17b}$$

$$V_{\text{MnCO}_3}\, \frac{\partial C_{\text{MnCO}_3}(z)}{\partial z} = K_3^{\text{Mn}}\, C_{\text{MnO}_2}(z) \\ - K_4^{\text{Mn}}(C_{\text{MnCO}_3}(z))^{1.7}, \tag{17c}$$

$$V_{\text{MnCO}_3}\, \frac{\partial C_{\text{MnCO}_3}(z)}{\partial z} = -K_4^{\text{Mn}}(C_{\text{MnCO}_3}(z))^{1.7}, \tag{17d}$$

$$V_{\text{MnS}_2}\, \frac{\partial C_{\text{MnS}_2}(z)}{\partial z} = K_5^{\text{Mn}}(C_{\text{MnCO}_3}(z))^{1.7}. \tag{17e}$$

While Eq. (17a) is applied for the suboxic layer, Eqs. (17b) and (17c) are applied for the upper part of the anoxic layer and Eqs. (17d) and (17e) are applied at intermediate and lower depths of the anoxic zone.

Oxidation of dissolved Mn(II) by nitrate has been suggested in many sediment studies (see Oguz et al., 2001 for a review) and in the Black Sea (Murray et al., 1995). This process has never been confirmed by direct microbiological rate experiments in the Black Sea (B. Tebo, pers. comm.), but Ottley et al. (1997) demonstrated direct chemical reduction of nitrate by dissolved Fe(II) in laboratory experiments. An attempt to parameterize oxidation of dissolved Mn(II) by oxygen according to the reaction kinetics (Murray and Brewer, 1977)

$$\frac{\partial[\text{Mn(II)}]}{\partial t} = k[\text{Mn(II)}][\text{MnO}_2][\text{OH}^-]^2[\text{O}_2] \tag{18}$$

revealed that the usually traced concentrations and vertical distribution of oxygen in the suboxic zone (Murray et al., 1995) cannot support oxidation of manganese in the lower part of the suboxic zone, while nitrate can, if the reaction kinetics are parameterized as

$$\frac{\partial[\text{Mn(II)}]}{\partial t} = k[\text{Mn(II)}][\text{MnO}_2][\text{NO}_3^-]^{2/5}. \tag{19}$$

The role of MnO_2 in auto-catalytic oxidation of dissolved Mn(II) by oxygen, suggested by Murray and Brewer (1977), has been found to be important when nitrate is formally assumed as the oxidant of dissolved Mn(II) in reaction (15a). The effect of pH has not been detected. This might be due to the narrow range of pH values observed near the onset of dissolved Mn(II) over the sea during different cruises. The best results have been obtained if the rate of dissolved Mn(II) oxidation is parameterized in the form of Eqs. (16a) and (17a).

We have found that the rate of reduction of Mn(IV) oxide (Eq. (15b)) does not depend on the sulfide concentration in ambient waters. Similarly, the power of 1.7 has been found to provide the best results in parameterizing production and dissolution of particulate MnCO_3. This situation is usual for heterogeneous reactions, when diffusion controls the overall rate of the process, for example, and equations of chemical reaction imply the mass balance, rather than kinetics of a process (Stumm and Morgan, 1996).

The set of Eqs. (17a)–(17e) can be solved for the unknown rate constants $K_1^{\text{Mn}}, K_2^{\text{Mn}}, K_3^{\text{Mn}}, K_2^{\text{Mn}}, K_4^{\text{Mn}}$, and K_5^{Mn} representing the specific rates of Mn(IV) oxide production and dissolution, Mn(II) carbonate production and dissolution, and Mn(II) sulfide production, respectively. The value of K_1^{Mn} varies in the range of 0.0003–0.00084 $\text{d}^{-1}\text{nmol}^{-1.4}$. Its mean value is obtained as 0.00046 ± 0.0002 $\text{d}^{-1}\text{nmol}^{-1.4}$ (Table 1). The mean values of other rate constants are determined as $K_2^{\text{Mn}} = 2.3\,\text{d}^{-1}$, $K_3^{\text{Mn}} = 2.7\,\text{d}^{-1}$, $K_4^{\text{Mn}} = 3.8\,\text{d}^{-1}\,\text{nmol}^{-0.7}$, and $K_5^{\text{Mn}} = 0.014\,\text{d}^{-1}\,\text{nmol}^{-0.7}$ (Table 1).

These parameters are hard to be tested in the same simple way, as for iron (Fig. 11), because a system of the second-order differential equations cannot be analytically solved. Still, these parameters have been successfully applied to numerically simulate and investigate nitrogen reactions in the suboxic zone (Murray et al., 2003) and the redox budget and evolution of the suboxic zone in the Black Sea (Konovalov et al., 2003).

9. Discussion

The aim of this work is to provide deeper insights into iron and manganese cycling in the

suboxic   (~15.6 ≤ σ_t ≤ ~16.2)   and   anoxic (σ_t ≥ ~16.2) layers of the Black Sea water column. Contrary to our previous knowledge, these metals reflect different redox and dissolved-particulate element cycling. The residence time of dissolved iron, determined by the ratio of its inventory to its removal rate from the water column, is much shorter than that for dissolved manganese. The difference between the residence times suggests that the concentration of iron is very sensitive to its external flux into the Black Sea. As available data show a broad range of temporal variations in the atmospheric flux of iron at the sea surface (Mitropolsky et al., 1982), the 1.5-fold changes in the maximum concentrations of dissolved iron from 1988 to 1994 (Fig. 1a and b) provide evidence for its short residence time in the water column. The vertical distribution of dissolved manganese (Fig. 1c and d), on the other hand, appears to remain uniform for the same period reflecting its longer residence time.

The upward flux of dissolved iron (6.36×10^8 mol year^{-1}) at the onset of sulfide (Fig. 3a and b) is small when compared to the external influx of iron of 36×10^8 mol year^{-1}, as an equivalent to the mean deep-area integrated sedimentation rate of iron sulfides of 35 μmol m^{-2} d^{-1} (Muramoto et al., 1991). This is opposite to the case for manganese and may explain the absence of a maximum in the vertical distribution of suspended iron at the suboxic/ anoxic interface. As the downward flux of suspended oxidized species equals the sum of the upward flux of the dissolved form and the external flux, the maximum becomes detectable when the flux of the dissolved form exceeds its external flux a few-fold. This is true for manganese but not for iron.

The analysis of the production–consumption rates confirms net oxidation of dissolved manganese in the suboxic zone, which is an expected result from the redox potential of Mn(II)/Mn(IV). This is also true for iron. An intriguing feature of iron cycling is that a major part of the upward flux of dissolved iron is removed below the onset of sulfide suggesting oxidation of dissolved iron inside the anoxic zone (Fig. 3). We believe this occurs due to oxidation of dissolved Fe(II) by

suspended Mn(IV), as has been suggested for ground waters (Postma, 1985) and demonstrated in laboratory experiments (Postma and Appelo, 2000). This makes cycling of iron in the Black Sea suboxic–anoxic water column highly dependent on cycling of manganese, rather than being independent. Redox cycling of manganese, on the other hand, is nearly independent of the cycling of iron, as only 1% of the flux of suspended Mn(IV) oxide is needed to oxidize Fe(II).

The analysis of the downward flux of particulate iron and manganese has revealed additional differences in cycling of these elements in the anoxic water column. We found that two particulate species of iron are needed to explain the vertical profile of suspended iron (Fig. 12), while three particulate species are necessary to parameterize the profile of suspended manganese (Fig. 13). The two forms of suspended iron are proposed to be Fe(III) hydroxide and iron sulfide. We do believe that iron sulfide undergoes a sequence of transformations to finally form pyrite (Rickard, 1997; Rickard and Luther, 1997), but available data on the vertical distribution of particulate iron and temporal variations in the external flux of iron to the Black Sea are not sufficient to resolve and parameterize these processes. In addition to Mn(III, IV) oxides and manganese sulfide, it was found that another (third) form of suspended manganese should exist to explain the calculated sharp increase in the rate of sinking of suspended manganese from about 15 to almost 200 m d^{-1} (Fig. 6). This suspended form has been attributed to manganese carbonate, which might exist as an individual solid phase for the conditions of the observed concentrations of dissolved Mn(II) and carbonate (Spencer and Brewer, 1971). We expect it to be formed in the upper part of the anoxic zone, then to sink and dissolve in deeper layers as the concentration of dissolved manganese decreases two-fold toward the bottom (Fig. 1c and d) and ambient waters become undersaturated with respect to manganese carbonate. Sinking MnCO$_3$ provides an effective downward flux of manganese that compensates the upward flux of dissolved manganese and flux of manganese sulfide from the water column. This maintains rather high concentrations of dissolved
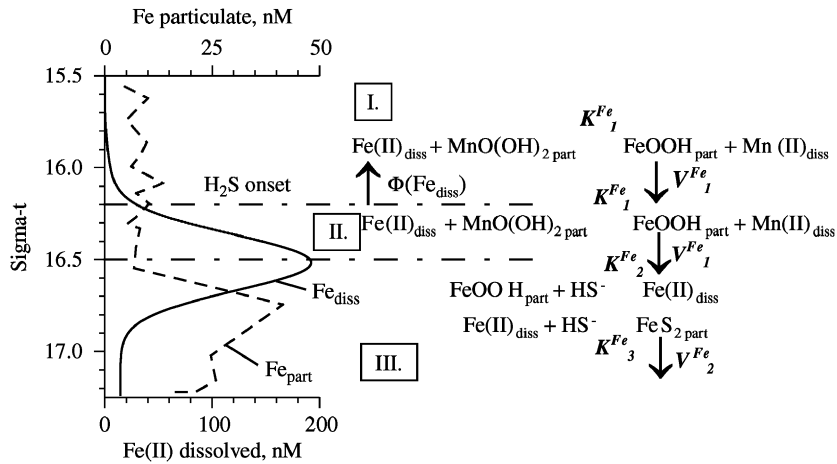
Fig. 12. Scheme of the parameterizations of iron cycling in the suboxic–anoxic water column of the Black Sea.
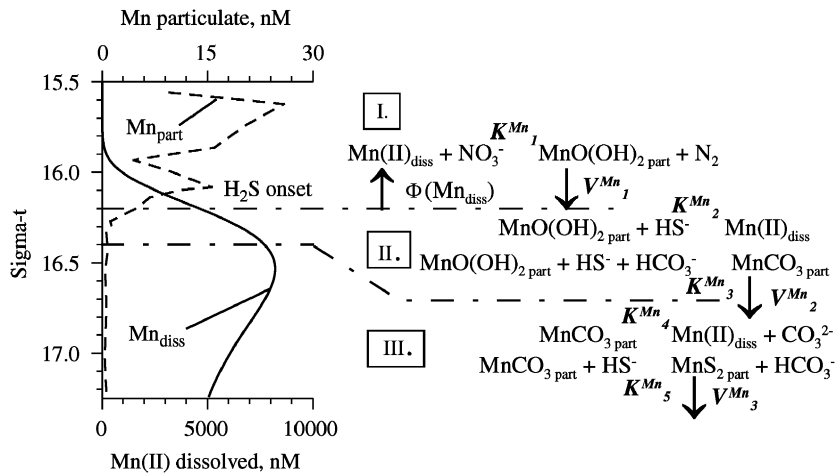

Fig. 13. Scheme of the parameterizations of manganese cycling in the suboxic–anoxic water column of the Black Sea.

manganese in the middle and deep part of the anoxic zone. Fe(II) carbonate is not formed as the ion activity product is lower than the conventional solubility product. The downward flux of dissolved iron rapidly expires above $\sigma_t \sim 16.7\,\mathrm{kg\,m^{-3}}$ to form suspended iron sulfide. Thus, solubility of iron sulfide controls the concentration of dissolved iron at a very low level in the anoxic zone below $\sigma_t \sim 16.7\,\mathrm{kg\,m^{-3}}$, while dissolution of manganese carbonate keeps the concentration of dissolved manganese at a higher level, as compared to dissolved iron.

An overall scheme of the processes, as schematically shown in Figs. 12 and 13 for iron and manganese cycling, respectively, suggests three individual layers for both of these metals. Layer I, above the sulfide onset ($\sigma_t = 16.2\,\mathrm{kg\,m^{-3}}$) is the suboxic layer. It is dominated by oxidation of dissolved Mn(II) and Fe(II). Data are fit best when nitrate is assumed to oxidize dissolved Mn(II) to Mn(III, IV) oxides, which in turn oxidize dissolved Fe(II). Layer II, the upper part of the anoxic zone, is the site of reactions dealing with reduction and dissolution of suspended Fe(III) and Mn(III, IV)

oxides. It is also the layer of active oxidation of dissolved Fe(II) by Mn(III, IV) oxides and the layer of production of suspended $MnCO_3$. Particulate Fe(II) carbonate does not exist as the concentration of dissolved iron is about 1/30 of that for dissolved manganese. The ion activity product is lower than the conventional solubility product and water remains undersaturated with respect to Fe(II) carbonate. Layer III, the deeper part of the anoxic zone, is the layer of precipitation of sulfides of manganese and iron, but fast sinking of $MnCO_3$ at a rate of about $200\,\mathrm{m\,d^{-1}}$ provides an effective downward flux of manganese, while the downward flux of dissolved iron is limited to the middle part of the anoxic zone to generate the flux of iron sulfide.

Acknowledgements

References

Bacon, M.P., Brewer, P.G., Spencer, D.W., Murray, J.W., Goddard, J.D., 1980. Lead-210, polonium-210, manganese and iron in the Cariaco Trench. Deep-Sea Research 27, 119–135.

Brewer, P.G., Spencer, D.W., 1971. Colorimetric determination of manganese in anoxic waters. Limnology and Oceanography 16, 107–112.

Buesseler, K.O., Livingston, H.D., Ivanov, L., Romanov, A., 1994. Stability of the oxic/anoxic interface in the Black Sea. Deep-Sea Research I 41, 283–296.

Codispoti, L.A., Friederich, G.E., Murray, J.W., Sakamoto, C.M., 1991. Chemical variability in the Black Sea: implications of continuous vertical profiles that penetrated the oxic/anoxic interface. Deep-Sea Research 38 (Suppl. 2a), S691–S710.

Diercks, A.-R., Asper, V.L., 1997. In situ settling speeds of marine snow aggregates below the mixed layer: Black Sea and Gulf of Mexico. Deep-Sea Research I 44 (3), 385–398.

Grasshoff, K., Ehrhardt, M., Kremling, K. (with contribution by Almgren, T., Andreae, M.O., Dawson, R., Duinker, J.C., Dyrssen, D., Ehrhardt, M., Fonselius, S., Grasshoff, K., Hansen, H.P., Hillebrand, Th., Josefsson, B., Koroleff, F., Kremling, K., Liebezeit, G., Olafsson, J., Statham, P.J., Williams, P.J.LeB.), 1983. Methods of Seawater Analysis. second, revised and extended ed. Verlag Chemie GmbH, D-6940 Weinheim, pp. 239–244.

Ivanov, L.I., Samodurov, A.S., 2001. The role of lateral fluxes in ventilation of the Black Sea. Journal of Marine Systems 32, 159–174.

Karl, D.M., Knauer, G.A., 1991. Microbial production and particle flux in the upper 350 m of the Black Sea. Deep-Sea Research 38 (Suppl. 2A), S655–S661.

Konovalov, S., Tugrul, S., Basturk, O., Salihoglu, I., 1997. Spatial isopycnal analysis of the main pycnocline chemistry of the Black Sea: seasonal and interannual variations. In: Ozsoy, E., Mikaelyan, A. (Eds.), Sensitivity to Change: Black Sea, Baltic Sea and North Sea, vol. 27. NATO ASI Series 2: Environment. Kluwer Academic Publishers, Dordrecht, The Netherlands, pp. 197–210.

Konovalov, S.K., Murray, J.W., Luther, G.W., Buesseler, K.O., Friederich, G., Tebo, B.M., Samodurov, A.S., Gregoire, M., Ivanov, L.I., Romanov, A.S., Clement, B., Murray, K., 2003. Oxygen fluxes, redox processes and the suboxic zone in the Black Sea. Proceeding of the Second International Conference on Oceanography of the Eastern Mediterranean and the Black Sea, Ankara, Turkey, 14–18 October 2002. TUBITAK Publishers, pp. 566–577.

Kremling, K., 1983. The behavior of Zn, Cd, Cu, Ni, Co, Fe and Mn in anoxic Baltic waters. Marine Chemistry 13, 87–108.

Landing, W.M., Lewis, B.L., 1991. Thermodynamic modeling of trace metal speciation in the Black Sea. In: Izdar, E., Murray, J.W. (Eds.), Black Sea Oceanography. Kluwer Academic Publishers, Dordrecht, The Netherlands, pp. 125–160.

Landing, W.M., Westerlund, S., 1988. The solution chemistry of iron (II) in Framvaren Fjord. Marine Chemistry 23, 329–343.

Lewis, B.L., Landing, W.M., 1991. The biogeochemistry of manganese and iron in the Black Sea. Deep-Sea Research 38 (Suppl. 2A), S773–S804.

Mitropolsky, A.Yu., Bezborodov, A.A., Ovsyany, E.I., 1982. Geokhimiya Chernogo morya (Hydrochemistry of the Black Sea). Naukova Dumka, Kiev, 144pp (in Russian).

Muramoto, J., Honjo, S., Fry, B., Hay, B.J., Howarth, R.W., Cisne, J.L., 1991. Sulfur, iron and organic carbon fluxes in the Black Sea: sulfur isotopic evidence for origin of sulfur fluxes. Deep-Sea Research 38 (Suppl. 2A), S1151–S1188.

Murray, J.W., Brewer, P.G., 1977. Mechanisms of removal of manganese, iron and other trace metals from sea water. Marine Manganese Deposits, Elsevier Oceanographic Series 15, 291–325 (Chapter 10).

Murray, J.W., Codispoti, L.A., Friederich, G.E., 1995. Oxidation–reduction environments. The suboxic zone in the Black Sea. In: Huang, C.P., O'Melia, C.R., Morgan, J.J. (Eds.), Aquatic Chemistry: Interfacial and Interspecies Processes. ACS Advances in Chemistry Series 244, 157–176.

Murray, J.W., Lee, B.S., Luther III, G.W., 1999. The suboxic zone of the Black Sea. In: Besiktepe, S., Unluata, U., Bologa, A. (Eds.), Environmental Degradation of the Black Sea: Challenges and Remedies, vol. 56. NATO ASI Series 2. Kluwer Academic Publishers, Dordrecht, The Netherlands, pp. 75–92.

Murray, J.W., Konovalov, S.K., Callahan, A., 2003. Nitrogen reactions in the suboxic zone of the Black Sea: new data and models based on the KNORR 2001 cruise. Proceeding of the Second International Conference on Oceanography of the Eastern Mediterranean and the Black Sea, Ankara, Turkey, 14–18 October 2002. TUBITAK Publishers, pp. 591–602.

Oguz, T., Murray, J.W., Callahan, A., 2001. Modeling redox cycling across the suboxic–anoxic interface zone in the Black Sea. Deep-Sea Research I 48, 761–787.

Ottley, C.J., Davison, W., Edmunds, W.M., 1997. Chemical catalysis of nitrate reduction by iron (II). Geochimica et Cosmochimica Acta 61 (9), 1819–1828.

Postma, D., 1985. Concentration of Mn and separation from Fe in sediments—I. Kinetics and stoichiometry of the reaction between birnessite and dissolved Fe(II) at 10 °C. Geochimica et Cosmochimica Acta 49, 1023–1033.

Postma, D., Appelo, C.A.J., 2000. Reduction of Mn-oxides by ferrous iron in a flow system: column experiment and reactive transport modeling. Geochimica et Cosmochimica Acta 64 (7), 1237–1247.

Rickard, D., 1997. Kinetics of pyrite formation by the H_2S oxidation of iron (II) monosulfide in aqueous solutions between 25 and 125 °C: the rate equation. Geochimica et Cosmochimica Acta 61 (1), 115–134.

Rickard, D., Luther, G.W., 1997. Kinetics of pyrite formation by the H2S oxidation of iron (II) monosulfide in aqueous solutions between 25 and 125 °C: the mechanism. Geochimica et Cosmochimica Acta 61 (1), 135–147.

Samodurov, A.S., Ivanov, L.I., 1998. Processes of ventilation of the Black Sea related to water exchange through the Bosporus. In: Ivanov, L., Oguz, T. (Eds.), NATO TU-Black Sea Project Ecosystem Modeling as a Management Tool for the Black Sea, Symposium on Scientific Results, vol. 2/47, no. 2. NATO ASI Series. Kluwer Academic Publishers, Dordrecht, The Netherlands, pp. 221–235.

Saydam, C., Tugrul, S., Basturk, O., Oguz, T., 1993. Identification of the oxic/anoxic interface by isopycnal surfaces in the Black Sea. Deep-Sea Research I 40, 1405–1412.

Spencer, D.W., Brewer, P.G., 1971. Vertical advection, diffusion and redox potentials as controls on the distribution of manganese and other trace metals dissolved in waters of the Black Sea. Journal of Geophysical Research 76, 5877–5892.

Spencer, D.W., Brewer, P.G., Sachs, P.L., 1972. Aspects of the distribution and trace element composition of suspended matter in the Black Sea. Geochimica et Cosmochimica Acta 36, 71–86.

Stumm, W., Morgan, J.J., 1996. Aquatic Chemistry: Chemical Equilibria and Rates in Natural Waters, third ed. A Wiley-Interscience Publication, New York, pp. 61–81.

Tebo, B.M., 1991. Manganese (II) oxidation in the suboxic zone of the Black Sea. Deep-Sea Research 38 (Suppl. 2A), S883–S906.

Tugrul, S., Basturk, O., Saydam, C., Yilmaz, A., 1992. The use of water density values as a label of chemical depth in the Black Sea. Nature 359, 137–139.

Vinogradov, M.E., Nalbandov, Yu.R., 1990. Vliyanie izmeneniya plotnosti vodi na raspredelenie phizicheskikh, khimicheskikh i biologicheskikh kharakteristik ekosistemi Chernogo morya (The influence of the variations in density of water at the distribution of physical, chemical, and biological properties of the Black Sea ecosystem). Okeanologiya (Oceanology) 30 (5), 769–777 (in Russian).

Zhang, J-Z., Millero, F.J., 1993. The chemistry of the anoxic waters in the Cariaco Trench. Deep-Sea Research I 40 (5), 1023–1041.